



Structure reinvestigation of α -, β - and γ - In_2S_3

Paul Pistor,^{a,*‡} Jose M. Merino Álvarez,^b Máximo León,^b Marco di Michiel,^c Susan Schorr,^{a,d} Reiner Klenk^a and Sebastian Lehmann^e

^aHelmholtz-Zentrum Berlin, Germany, ^bApplied Physics Department, Universidad Autónoma de Madrid, Spain, ^cESRF – The European Synchrotron, Grenoble, France, ^dFreie Universität Berlin, Berlin, Germany, and ^eSolid State Physics, Lund University, Sweden. *Correspondence e-mail: ppistor@irec.cat

Received 27 January 2016

Accepted 26 April 2016

Edited by P. Bordet, Institut Néel, France

‡ Current address: IREC – Catalonia Institute for Energy Research, Sant Adrià de Besòs, Spain.

Keywords: indium sulfide; In_2S_3 ; tetragonal; cubic; trigonal; crystal structure analysis; lattice parameter; Rietveld refinement; thermal expansion coefficient; high temperature.

CCDC references: 1476600; 1481751; 1481752

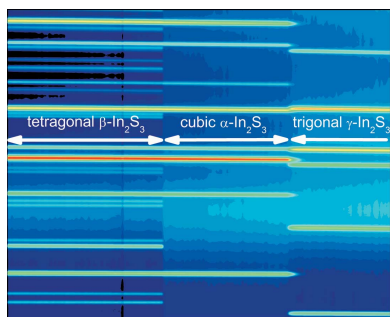
Supporting information: this article has supporting information at journals.iucr.org/b

Semiconducting indium sulfide (In_2S_3) has recently attracted considerable attention as a buffer material in the field of thin film photovoltaics. Compared with this growing interest, however, detailed characterizations of the crystal structure of this material are rather scarce and controversial. In order to close this gap, we have carried out a reinvestigation of the crystal structure of this material with an *in situ* X-ray diffraction study as a function of temperature using monochromatic synchrotron radiation. For the purpose of this study, high quality polycrystalline In_2S_3 material with nominally stoichiometric composition was synthesized at high temperatures. We found three modifications of In_2S_3 in the temperature range between 300 and 1300 K, with structural phase transitions at temperatures of 717 K and above 1049 K. By Rietveld refinement we extracted the crystal structure data and the temperature coefficients of the lattice constants for all three phases, including a high-temperature trigonal γ - In_2S_3 modification.

1. Introduction

In_2S_3 is a widegap semiconductor with high photoconductive and photoluminescent properties, which makes it a promising material for optoelectronic applications (Shazly *et al.*, 1998). Most prominently, its potential application as a buffer layer in chalcopyrite solar cells has triggered an increased research effort in its fundamental materials properties (*e.g.* crystal structure, optical properties, electronic bandstructure *etc.*) as well as in deposition technology. The compatibility with various thin film deposition methods make it a versatile alternative to the commonly applied CdS buffer layer. Among the compatible deposition methods, atomic layer deposition (Naghavi *et al.*, 2003), the ion layer gas reaction (ILGAR) method (Sáez-Araoz *et al.*, 2012), spray pyrolysis (John *et al.*, 2005), sputtering (Hariskos *et al.*, 2005) and evaporation (Strohm *et al.*, 2005) have been successfully applied. The interested reader is referred here to the excellent review by Barreau (2009) on the role of In_2S_3 in the world of photovoltaics. Various reports on In_2S_3 buffer layers correlate deposition process parameters with crystallographic properties (Rao & Kumar, 2012; Larina *et al.*, 2004; Yoosuf & Jayaraj, 2005) and ultimately with final solar cell device parameters (Naghavi *et al.*, 2003; Pistor, Caballero *et al.*, 2009).

For a correct interpretation of the crystallographic data, a comprehensive understanding of the relevant crystal structure modifications of In_2S_3 is mandatory. Data reported on the phase labelling and temperature sequence in the In–S system is contradictory. In view of recent technological and scientific interest in In_2S_3 and the commonly drawn connection to its crystal structure properties, in this contribution we therefore



OPEN  ACCESS

report about a crystal structure reinvestigation of the In_2S_3 system in the temperature range from room temperature up to 1322 K, close to the melting point at 1363 K (Diehl *et al.*, 1976). The present study results in high quality reference powder diffraction data sets and enhanced knowledge on the different structure modifications of In_2S_3 , which is expected to have a direct impact on the technological understanding in terms of *e.g.* material quality or diffusion parameters.

The first to describe the crystal structure of In_2S_3 were Hahn & Klingler (1949). They reported a cubic phase at temperatures below 600 K, which they called $\alpha\text{-In}_2\text{S}_3$ and a transition to a tetragonal spinel-like high-temperature modification which they called $\beta\text{-In}_2\text{S}_3$. They already stressed the similarity between both modifications and suggested an ordering of the In atoms to be the main difference between the two phases. Later studies revealed that the cubic phase is in fact the higher-temperature phase and the stoichiometric phase existing at room temperature is tetragonal. However, for sulfur-deficient In_2S_3 the temperature range for the cubic phase extends down to room temperature. So Hahn probably measured a sulfur-deficient cubic $\alpha\text{-In}_2\text{S}_3$ at room temperature and called it the lower temperature modification and from here most confusion about the labelling and temperature sequence of phases arises.

While the majority of authors follow Hahn in their nomenclature resulting in an ordering of the phases from low to high temperature as $\beta\text{-}\alpha\text{-}\gamma$, some have relabeled the cubic and tetragonal phase with a resulting order of $\alpha\text{-}\beta\text{-}\gamma$. Depending on the author, $\beta\text{-In}_2\text{S}_3$ in recent publications may therefore refer either to the low-temperature tetragonal phase or the cubic high-temperature phase. Although $\alpha\text{-}\beta\text{-}\gamma$ would be the logical order, we will follow the majority in the literature and assign $\beta\text{-In}_2\text{S}_3$ to the low-temperature, tetragonal phase.

There are some more and sometimes contradictory publications in the literature on the crystal structure of the different In_2S_3 phases, of which the most relevant ones will be shortly introduced in the following. Gödecke & Schubert (1985) suggest a phase diagram in which for the In:S ratio of 2:3 three modifications ($\beta\text{-In}_2\text{S}_3$, $\alpha\text{-In}_2\text{S}_3$ and $\gamma\text{-In}_2\text{S}_3$) of indium sulfide exist in three different temperature regimes. King (1962) determined the space group of the tetragonal $\beta\text{-In}_2\text{S}_3$ as $I4_1/amd$ (space group No. 141) and the lattice parameters to $a_0 = 7.61 \text{ \AA}$ and $c_0 = 32.24 \text{ \AA}$ using Weissenberg photographs. The space group was later confirmed by Goodyear & Steigmann (1961) and Steigmann *et al.* (1965) who reported the lattice parameters as $a_0 = 7.623 \text{ \AA}$ and $c_0 = 32.36 \text{ \AA}$. Hahn described the space group of the cubic $\alpha\text{-In}_2\text{S}_3$ as $Fd\bar{3}m$, with a lattice parameter of 10.72 \AA (Hahn & Klingler, 1949). The high-temperature $\gamma\text{-In}_2\text{S}_3$ modification has not been characterized in detail yet since a quenching to room temperature conditions was not successful (Diehl *et al.*, 1976). However, Diehl *et al.* succeeded in synthesizing a modified $\gamma\text{-In}_2\text{S}_3$ phase with an additional 5 at. % of As or Sb stabilizing it at room temperature. For this modified trigonal $\gamma\text{-In}_2\text{S}_3$ they suggested a space group of $P\bar{3}m1$ with lattice parameters a_0 between 3.806 and 3.831 \AA and c_0 between 9.044 and 9.049 \AA .

Some recent publications refer to the thin film application of In_2S_3 and cite X-ray diffraction (XRD) database information. An assignment to the tetragonal $\beta\text{-In}_2\text{S}_3$ is often made although the quality of the diffraction data for In_2S_3 is generally poor and does not allow for a definite distinction between the tetragonal $\beta\text{-In}_2\text{S}_3$ and the cubic $\alpha\text{-In}_2\text{S}_3$. A correct distinction between the two phases would however allow for a verification of the film stoichiometry, as the $\beta\text{-In}_2\text{S}_3$ only exists in a very small stoichiometry range (Gödecke & Schubert, 1985). It is the scope of this work to reinvestigate the In_2S_3 in view of these aspects and to present a clear and detailed description of its crystal structure over the temperature range from room temperature to above 1300 K.

2. Experimental methods

2.1. Sample preparation

Indium sulfide was synthesized by heating weighted stoichiometric amounts of sulfur and indium in the ratio 3:2 in evacuated quartz ampoules. Source materials were indium granulate (> 99.999% purity) and sulfur flakes (> 99.999% purity). An excess of 4 atomic percent of S was provided for two reasons: (i) to account for sulfur losses during the preparation; (ii) the excess sulfur is not incorporated into the crystal structure according to the phase diagram (Gödecke & Schubert, 1985). The weighted source materials were filled in a graphite boat and placed in a quartz glass ampoule, evacuated ($< 10^{-3}$ mbar) and sealed. The ampoule was placed in a two-zone oven and heated above the melting point to 1373 K for 24 h to enable the complete sulfurization of the indium. To assure that the synthesis was completed, the ampoule was then kept at 1073 K for 2 d, at 873 K for 2 d and at 673 K for 4 d. The synthesized indium sulfide was manually ground in a mortar before XRD measurements and had a brick red appearance.

2.2. Diffraction measurement

For the diffraction measurement, ground indium sulfide powder was sealed in a quartz glass ampoule. The XRD measurements were performed at the ESRF, the European Synchrotron, Grenoble, France, at the beamline ID15B using monochromatic high-energy synchrotron light with a wavelength of 0.14276 \AA . XRD patterns were recorded every 5 K, while heating the sample from 304 to 1322 K with a constant heating rate of 300 K h^{-1} . The detector type used was a Pixium 4700, the detector-to-sample distance was 1037.132 mm, and the furnace was a resistively heated tube furnace.

2.3. Details of the Rietveld refinement

The software *FullProf Suite* (February 2016 version) was used for the Rietveld refinement of the recorded diffractograms (Rodríguez-Carvajal, 2001). Apart from 7 profile parameters, the lattice parameters were fitted, as well as the atomic position coordinate parameters where appropriate, the isotropic temperature factor for all atomic positions, and the

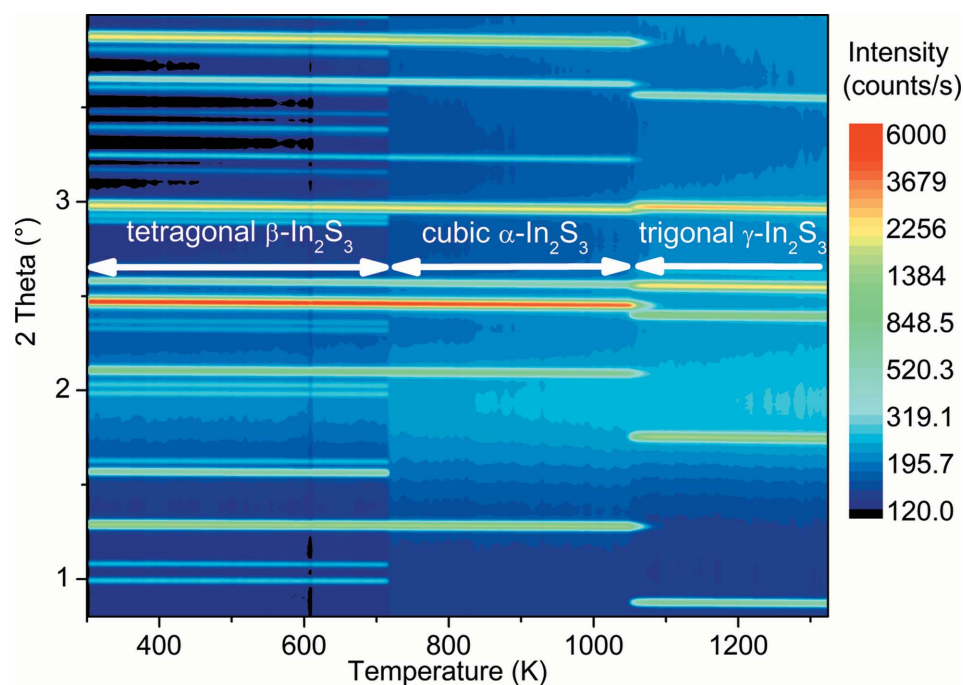


Figure 1 Map of temperature-dependent X-ray diffractograms (XRD) for the In_2S_3 powder. Each diffractogram is measured at a specific temperature which corresponds to one column in the graph with the y-direction displaying the 2θ diffraction angle. The position of the column in the x-direction corresponds to the temperature at which the diffractogram was recorded, while the colour indicates the XRD intensity in logarithmic scale (dark blue = low intensity, red = high intensity). Three structural modifications of In_2S_3 in different temperature regimes can be distinguished according to appearing/disappearing diffraction peaks as indicated in the figure. The wavelength of the incident X-ray photons is 0.14276 Å.

Table 1 Lattice parameters as extracted from the Rietveld refinement for the three In_2S_3 modifications.

	Temperature (K)	Space group	Number	$a_0 = b_0$ (Å)	c_0 (Å)	$\alpha = \beta$ (°)	γ (°)	
#1	$\beta\text{-In}_2\text{S}_3$	309	$I4_1/amd$	141	7.6231 (4)	32.358 (3)	90	90
#2	$\alpha\text{-In}_2\text{S}_3$	749	$Fd\bar{3}m$	227	10.8315 (2)	10.8315 (2)	90	90
#3	$\gamma\text{-In}_2\text{S}_3$	1099	$P\bar{3}m1$	164	3.8656 (2)	9.1569 (5)	90	120

Table 2 Refinement parameters for the Rietveld refinements performed for the three modifications of In_2S_3 .

R_B : Bragg R_I factor, χ_v^2 : χ^2 for points with Bragg contribution, R_{wp} : weighted profile R -factor (not corrected for background), R_{exp} : expected R -factor (not corrected for background), cR_{wp} : weighted profile R factor (corrected for background), cR_{exp} : expected R -factor (corrected for background), $\text{Ratio}_{h/p}$: ratio between effective number of reflections and intensity parameters.

	Temperature (K)	χ_v^2	R_B	R_{wp}	R_{exp}	cR_{wp}	cR_{exp}	$\text{Ratio}_{h/p}$	
#1	$\beta\text{-In}_2\text{S}_3$	309	10.4	0.014	0.031	0.01	0.049	0.015	5.9
#2	$\alpha\text{-In}_2\text{S}_3$	749	7.9	0.017	0.028	0.01	0.055	0.020	7.3
#3	$\gamma\text{-In}_2\text{S}_3$	1099	10.8	0.028	0.030	0.01	0.072	0.024	3.8

occupational factors of the indium positions. In addition we fitted the background by a list of manually inserted points which will add to the list of refined parameters.

3–5, respectively. For all three phases we obtained a good agreement between measurement and simulation with χ^2 values below 11 and Bragg R_I -factors below 0.03. More

3. Results

3.1. Temperature-dependent phase analysis

In_2S_3 powder was prepared from the elements *via* a high-temperature route as described in §2.1. The mortared In_2S_3 powder was filled into quartz glass ampoules which were instantaneously evacuated and sealed. The X-ray diffractograms were recorded in the temperature range from 304 to 1322 K, and details on the diffraction measurements can be found in §2.2. A color scale map of all diffractograms is depicted in Fig. 1. In this graph, color indicates the counts and the three temperature ranges corresponding to the three different phases with distinct diffraction patterns can be well separated. We find a sharp structural phase transition between the first two phases at a temperature of 717 ± 5 K. This transition is characterized by the disappearance of several minor intensity diffraction peaks, while the main diffraction peak positions and intensities remain approximately constant for both phases (see Figs. 1 and 2). A second transition was observed in the temperature range between 1049 and 1084 K. Here, all peaks of the $\alpha\text{-In}_2\text{S}_3$ disappear and are replaced by the diffraction peaks of $\gamma\text{-In}_2\text{S}_3$ indicating a complete reordering of the atoms in the crystal structure.

3.2. Rietveld refinement of the three In_2S_3 modifications

We carried out full Rietveld refinements of the three diffractograms recorded at temperatures of 309, 749 and 1099 K. The refined lattice parameters are listed in Table 1. The three diffractograms, refinements and residues are displayed in Fig. 2. The calculated figures of merit and atomic positions can be found in Tables 2 and

detailed information on the refinement parameters are included in the CIF file in the supporting information.

3.3. Temperature dependence of the lattice parameters

Finally, the XRD data measured at different temperatures have been processed in batch-mode Rietveld refinements to extract the temperature dependence of the relevant lattice parameters. An example is shown in Fig. 3 for the lattice parameter a_0 of the cubic α - In_2S_3 phase in the temperature range between 749 and 1044 K. The data are well fitted with the linear fit function

$$a(T) = 10.7480 \text{ \AA} + 1.121(2)T \times 10^{-4} \text{ \AA K}^{-1}.$$

From the temperature dependence of the lattice constants, we obtain the linear thermal expansion coefficient α

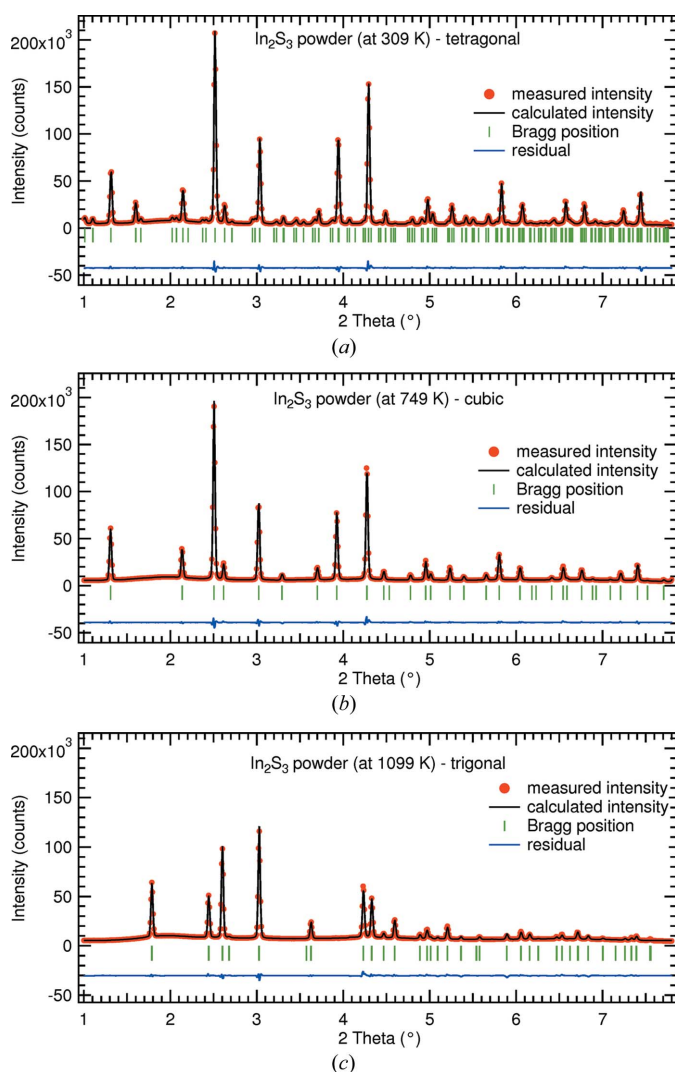


Figure 2 Diffraction data and Rietveld refinement of the three In_2S_3 modifications fully refined in this study. The displayed residua have been vertically shifted for better comparison. (a) Tetragonal modification measured at 309 K; (b) cubic modification measurement at 749 K; (c) trigonal modification measured at 1099 K.

Table 3

Atomic sites for the tetragonal β - In_2S_3 , (space group 141, origin choice No. 2).

Atom	Wickoff	x	y	z	U_{iso}	Occ.
S1	16h	0	-0.005 (2)	0.2513 (7)	0.013 (4)	1.0
S2	16h	0	0.008 (2)	0.0777 (7)	0.016 (4)	1.0
S3	16h	0	0.020 (2)	0.4133 (7)	0.015 (4)	1.0
In1	8e	0	1/4	0.2046 (2)	0.0097 (8)	0.973 (6)
In2	8c	0	0	0	0.0143 (15)	0.972 (7)
In3	16h	0	-0.0196 (3)	0.3327 (2)	0.0111 (10)	0.974 (6)

Table 4

Atomic sites for the cubic α - In_2S_3 (space group 227, origin choice No. 2).

Atom	Wickoff	x	y	z	U_{iso}	Occ.
S1	32e	0.2564 (2)	0.2564 (2)	0.2564 (2)	0.0347 (11)	1.0
In1	8a	1/8	1/8	1/8	0.0306 (9)	0.64 (4)
In2	16d	1/2	1/2	1/2	0.0445 (6)	0.978 (6)

Table 5

Atomic sites for the trigonal γ - In_2S_3 .

Atom	Wickoff	x	y	z	U_{iso}	Occ.
S1	2d	1/3	2/3	0.3359 (7)	0.054 (4)	1.0
S2	1a	0	0	0	0.091 (5)	1.0
In1	2d	1/3	2/3	0.8085 (3)	0.0510 (9)	0.829 (10)
In2	2d	1/3	2/3	0.6485 (12)	0.064 (6)	0.144 (3)

($\alpha_T = (da/dT)_T/a_T$; Kundra & Ali, 1976) for the cubic phase. In this temperature range, we calculate an average α of $10.3 \times 10^{-6} \text{ K}^{-1}$, in relatively good agreement with Kundra & Ali (1976), 10.8×10^{-6} – $10.9 \times 10^{-6} \text{ K}^{-1}$. The temperature dependence of the remaining lattice parameters of the tetragonal and trigonal phases are obtained accordingly and the fit functions are summarized in Table 6. For the tetragonal β - In_2S_3 we find an average linear expansion coefficient α in the a direction of $11.7 \times 10^{-6} \text{ K}^{-1}$ and in the c direction of $6.7 \times 10^{-6} \text{ K}^{-1}$. For the trigonal phase, an average linear expansion coefficient of $14.1 \times 10^{-6} \text{ K}^{-1}$ in the a direction and $26.7 \times 10^{-6} \text{ K}^{-1}$ in the c direction was determined.

4. Discussion

In this section we will briefly discuss the crystal structure of the three modifications and how the different modifications may impact the application of In_2S_3 in thin film solar cells.

The low-temperature modification β - In_2S_3 is best described with a defect spinel-type structure. The S atoms form a distorted cubic closed-spaced sublattice, in which the In atoms occupy the tetrahedral and octahedral interstitials the same way cations do in a regular spinel-like MgAl_2O_4 (Kleber *et al.*, 2002). While all the octahedral cation sites are occupied in β - In_2S_3 , one third of the tetrahedral sites remain unoccupied. For that reason the In_2S_3 structure is sometimes described in a quasi-ternary compound formula: $[\text{In}_{2/3}(\text{Vac})_{1/3}]^{\text{tet}}[\text{In}]_2^{\text{oct}}\text{S}_4$, where \square^{tet} and \square^{oct} denote tetrahedral and octahedral sites and (Vac) the vacancies. In β - In_2S_3 , the vacancies are ordered

Table 6
Linear fit function of the lattice parameters of In_2S_3 from the Rietveld refinements.

	Temperature range (K)	Fit function
#1 $\beta\text{-In}_2\text{S}_3$	309–704	$a = 7.5949 (2) \text{ \AA} + 8.967 (31)T \times 10^{-5} \text{ \AA K}^{-1}$ $c = 32.307 (2) \text{ \AA} + 1.607 (4)T \times 10^{-4} \text{ \AA K}^{-1}$
#2 $\alpha\text{-In}_2\text{S}_3$	749–1044	$a = 10.7480 (2) \text{ \AA} + 1.121 (2)T \times 10^{-4} \text{ \AA K}^{-1}$
#3 $\gamma\text{-In}_2\text{S}_3$	1099–1322	$a = 3.8044 (2) \text{ \AA} + 5.566 (15)T \times 10^{-5} \text{ \AA K}^{-1}$ $c = 8.877 (3) \text{ \AA} + 2.52 (2)T \times 10^{-4} \text{ \AA K}^{-1}$

along the 4_1 screw axis which is by definition parallel to the c -axis. The ordering of the vacancies gives rise to a small distortion of the cubic symmetry of the regular spinel structure. This small distortion is the origin of the tetragonal structure of the $\beta\text{-In}_2\text{S}_3$ with lower symmetry and leads to the additional peaks observed in the X-ray diffraction. Fig. 4

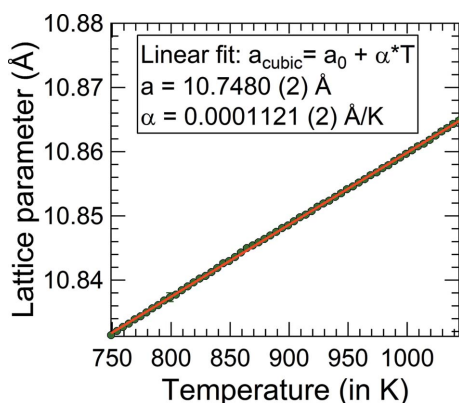


Figure 3
Temperature dependence of the lattice parameter for the cubic $\alpha\text{-In}_2\text{S}_3$. The resulting fit parameters of a linear fit are listed in the inset.

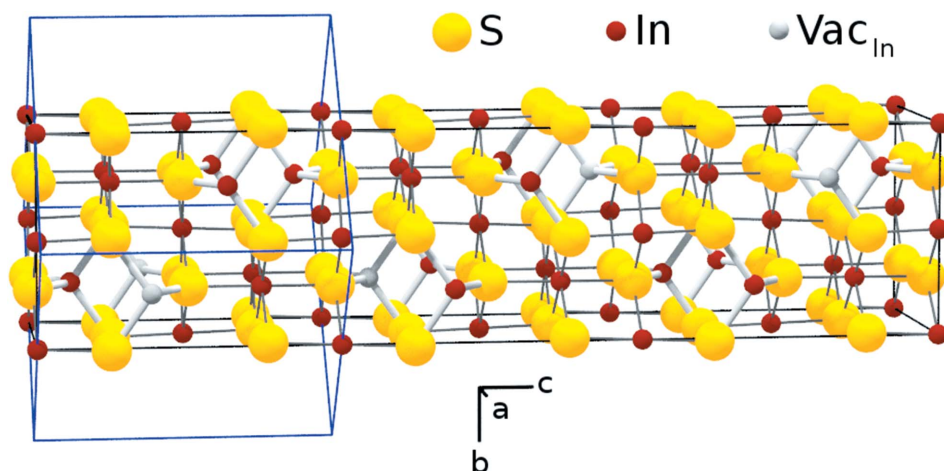


Figure 4
Structure model of a $\beta\text{-In}_2\text{S}_3$ unit cell. The tetrahedral bonds are drawn thicker for better identification. The indium vacancies are marked as grey spheres. In the tetragonal $\beta\text{-In}_2\text{S}_3$ configuration, the vacancies are ordered on a 4_1 screw axis parallel to the c -axis of the crystal. In the $\alpha\text{-In}_2\text{S}_3$ configuration, the vacancies are randomly distributed over all tetrahedral indium sites. The edges of the unit cell of the tetragonal $\beta\text{-In}_2\text{S}_3$ structure (cubic $\alpha\text{-In}_2\text{S}_3$) structure are indicated by black (blue) lines.

shows a plot of the $\beta\text{-In}_2\text{S}_3$ crystal structure based on the results obtained by the Rietveld refinement.

The transition from $\beta\text{-In}_2\text{S}_3$ to $\alpha\text{-In}_2\text{S}_3$ is an order–disorder transition. In $\alpha\text{-In}_2\text{S}_3$, the indium vacancies are randomly distributed over all tetrahedral sites, in contrast to the ordered configuration of vacancies in the $\beta\text{-In}_2\text{S}_3$. As a result of the disordering, $\alpha\text{-In}_2\text{S}_3$ adopts a cubic crystal structure. The resulting higher crystal symmetry explains the observed disappearance of some of the minor intensity peaks in the diffractograms at the transition from $\beta\text{-In}_2\text{S}_3$ to $\alpha\text{-In}_2\text{S}_3$ at 717 K.

Finally, the $\gamma\text{-In}_2\text{S}_3$ can be described as a layered structure as suggested by Diehl *et al.* and Bartzokas *et al.* (Diehl *et al.*, 1976; Bartzokas *et al.*, 1978). Here, the S atoms remain in a nearly closed-packed sublattice while the In atoms are exclusively found on octahedral sites forming a layered structure of subsequent S–In–S–In–S slabs.

The defect spinel-type structure of the $\beta\text{-In}_2\text{S}_3$ and $\alpha\text{-In}_2\text{S}_3$ has a direct phenomenological and technological impact. Because of the large number of natural vacancies in the structure, In_2S_3 can host various other atoms such as Na or Cu within its original lattice configuration (Barreau *et al.*, 2006). Both have been found to diffuse efficiently through In_2S_3 thin films (Pistor, Allsop *et al.*, 2009; Juma, Pistor *et al.*, 2012; Juma, Kavalakkatt *et al.*, 2012). The diffusion phenomena at interfaces in thin film solar cells containing In_2S_3 have not yet been fully understood but might benefit from an in-depth knowledge of the crystal (vacancy) structure of In_2S_3 . Where XRD data of good quality exist, it is an easy task to distinguish between the tetragonal and cubic phase of In_2S_3 by an examination of the characteristic additional peaks only present for the $\beta\text{-In}_2\text{S}_3$. The differentiation between $\alpha\text{-In}_2\text{S}_3$ and $\beta\text{-In}_2\text{S}_3$ allows testing for stoichiometry, since the tetragonal phase only exists in a very small compositional range. According to Gödecke & Schubert (1985) and Diehl &

Nitsche (1975), the compositional range for the $\beta\text{-In}_2\text{S}_3$ is less than 1 at %. The addition of a very small amount of surplus indium effectively suppresses the ordering of the In vacancies and therefore the formation of the tetragonal $\beta\text{-In}_2\text{S}_3$ phase. As a consequence, the crystal structure of off-stoichiometric $\text{In}_{2+x}\text{S}_3$ remains in the cubic $\alpha\text{-In}_2\text{S}_3$ modification down to room temperature. This specific feature is used for example to check if In_2S_3 source material for an evaporation process is still within the described stoichiometry range (Pistor, Caballero *et al.*, 2009). Alike the distinction of polycrystalline powder material, this type of analysis tool would be rather desirable for the evaluation of In_2S_3 thin film material as well.

However, reasonable X-ray diffraction data are necessary to distinguish between the two very similar spectra in order to resolve the fine additional peaks, a criterion often not met for XRD patterns available on In_2S_3 thin films.

5. Conclusions

We provide a detailed crystal structure analysis of In_2S_3 over the entire temperature range from room temperature up to close to the melting point covering the three modifications β - In_2S_3 , α - In_2S_3 and γ - In_2S_3 . With this, we contribute to the comprehensive understanding of the different phases existent and their interdependence. The high-temperature phase γ - In_2S_3 has been analysed and refined for the first time in the pure phase. Finally we show how the detailed knowledge of the phase diagram and the different In_2S_3 modifications might have a direct impact on the technological use of In_2S_3 in applications such as buffer layer deposition in thin film solar cell production.

Acknowledgements

Partial financial support for this work by the European Commission under contract number FP-6-019757 (LARCIS) and grant agreement number GA 625840 (JumpKEST) as well as by the DAAD within the PPP-program Acciones Integradas Hispano-Alemanas under the Contract No. 314-Al-edr (HA2006-0025 spanish reference) is gratefully acknowledged. The authors are also grateful to ESRF – The European Synchrotron, Grenoble, France, for granted beamtime. We are grateful to Juan Rodriguez-Carvajal for developing the *Full-Prof* program and his advice on the refinement.

References

Barreau, N. (2009). *Solar Energy*, **83**, 363–371.

- Barreau, N., Deudon, C., Lafond, A., Gall, S. & Kessler, J. (2006). *Solar Energy Mater. Solar Cells*, **90**, 1840–1848.
- Bartzokas, D., Manolikas, C. & Spyridelis, J. (1978). *Phys. Status Solidi. (A)*, **47**, 459–467.
- Diehl, R., Carpentier, C.-D. & Nitsche, R. (1976). *Acta Cryst.* **B32**, 1257–1260.
- Diehl, R. & Nitsche, R. (1975). *J. Cryst. Growth*, **28**, 306–310.
- Gödecke, T. & Schubert, K. (1985). *Z. Metallkdd.* **76**, 358–364.
- Goodyear, J. & Steigmann, G. (1961). *Proc. Phys. Soc.* **78**, 491–495.
- Hahn, H. & Klingler, W. (1949). *Z. Anorg. Chem.* **260**, 97–109.
- Hariskos, D., Menner, R., Lotter, E., Spiering, S. & Powalla, M. (2005). 20th European Photovoltaic Solar Energy Conference, pp. 1713–1716. Barcelona, Spain.
- Juma, A., Kavalakkatt, J., Pistor, P., Latzel, B., Schwarzburg, K. & Dittrich, T. (2012). *Phys. Status Solidi. (A)*, **209**, 663–668.
- Juma, A., Pistor, P., Fengler, S., Dittrich, T. & Wendler, E. (2012). *Thin Solid Films*. In the press.
- King, G. S. D. (1962). *Acta Cryst.* **15**, 512.
- Kleber, W., Bautsch, H.-J., Bohm, J. & Klimm, D. (2002). *Einführung in die Kristallographie*. Oldenbourg Wissenschaftsverlag.
- Kundra, K. & Ali, S. (1976). *Phys. Status Solidi. (A)*, **36**, 517–525.
- Larina, L., Kim, K. H., Yoon, K. H., Konagai, M. & Ahn, B. T. (2004). *J. Electrochem. Soc.* **151**, C789–C792.
- Naghavi, N., Spiering, S., Powalla, M., Cavana, B. & Lincot, D. (2003). *Prog. Photovolt. Res. Appl.* **11**, 437–443.
- Pistor, P., Allsop, N., Braun, W., Caballero, R., Camus, C., Fischer, C.-H., Gorgoi, M., Grimm, A., Johnson, B., Kropp, T., Lauer, M., Lehmann, S., Mönig, H., Schorr, S., Weber, A. & Klenk, R. (2009). *Phys. Status Solidi A*, **206**, 1059–1062.
- Pistor, P., Caballero, R., Hariskos, D., Izquierdo-Roca, V., Wächter, R., Schorr, S. & Klenk, R. (2009). *Solar Energy Mater. Solar Cells*, **93**, 148–152.
- Rao, P. & Kumar, S. (2012). *Thin Solid Films*, **524**, 93–99.
- Rodriguez-Carvajal, J. (2001). *IUCr Newsl.* **26**, 12–19.
- Sáez-Araoz, R., Krammer, J., Harndt, S., Koehler, T., Krueger, M., Pistor, P., Jasenek, A., Hergert, F., Lux-Steiner, M. & Fischer, C. (2012). *Prog. Photovolt. Res. Appl.* **20**, 855–861.
- Shazly, A. A. E., Elhady, D., Metwally, H. & Seyam, M. (1998). *J. Phys. Condens. Matter*, **10**, 5943–5954.
- Steigmann, G. A., Sutherland, H. H. & Goodyear, J. (1965). *Acta Cryst.* **19**, 967–971.
- Strohm, A., Eisenmann, L., Gebhardt, R., Harding, A., Schlötzer, T., Abou-Ras, D. & Schock, H. (2005). *Thin Solid Films*, **480–481**, 162–167.
- John, T. T., Mathew, M., Sudhakartha, C., Vijayakumar, K. P., Abe, T. & Kashiwaba, Y. (2005). *Solar Energy Mater. Solar Cells*, **89**, 27–36.
- Yoosuf, R. & Jayaraj, M. (2005). *Solar Energy Mater. Solar Cells*, **89**, 85–94.